Ultra-high-frequency chaos in a time-delay electronic device with band-limited feedback

Lucas Illing[a] and Daniel J. Gauthier
Department of Physics and Center for Nonlinear and Complex Systems, Duke University, Durham, North Carolina 27708

(Received 24 April 2006; accepted 18 July 2006; published online 30 August 2006)

We report an experimental study of ultra-high-frequency chaotic dynamics generated in a delay-dynamical electronic device. It consists of a transistor-based nonlinearity, commercially-available amplifiers, and a transmission-line for feedback. The feedback is band-limited, allowing tuning of the characteristic time-scales of both the periodic and high-dimensional chaotic oscillations that can be generated with the device. As an example, periodic oscillations ranging from 48 to 913 MHz are demonstrated. We develop a model and use it to compare the experimentally observed Hopf bifurcation of the steady-state to existing theory [Illing and Gauthier, Physica D **210**, 180 (2005)]. We find good quantitative agreement of the predicted and the measured bifurcation threshold, bifurcation type and oscillation frequency. Numerical integration of the model yields quasiperiodic and high dimensional chaotic solutions (Lyapunov dimension ~13), which match qualitatively the observed device dynamics. © *2006 American Institute of Physics*. [DOI: 10.1063/1.2335814]

Time-delayed feedback occurs in many systems and is particularly important at high-speeds, where the time it takes signals to propagate through the device components is comparable to the time scale of the fluctuations. Hence, many fast systems are most accurately described by time-delay differential equations. A fascinating feature of such systems is that seemingly simple devices can show exceedingly complex dynamics. This has motivated the use of time-delay feedback devices in practical applications of chaos, such as chaos communications and ranging, for which microwave and radio-frequency oscillators are needed. As an example of such a device, we explore the dynamics of an electronic circuit that consists of a simple transistor-based nonlinearity and time-delayed feedback. Taking the band-limiting characteristics of the device components into account allows us to develop a simple model that captures many of the observed features. We compare the observed dynamics to both theory and numerical calculations and find good agreement.

I. INTRODUCTION

The generation of chaotic signals is well understood for low-speed circuits,[1] i.e., for devices with characteristic frequencies in the Hz or kHz range. However, there is considerable interest in generating high-speed chaos because of promising applications such as random signal radar/lidar,[2–5] random number generation,[6–8] and communications.[9–14]

Generating broadband chaotic signals in the radio-frequency (rf) regime is challenging because electronic components used in low-speed electronic circuits, such as operational amplifiers, are not readily available above a few GHz. Therefore, new techniques for chaos generation need to be explored. Furthermore, design issues arise at rf frequencies that do not exist at low speeds, such as proper circuit layout, proper isolation of power supply and active circuit elements, and non-negligible time delays due to signal propagation, to name just a few.

These challenges are in part the reason that, to date, the most successful schemes for generating broadband chaotic signals at GHz-frequencies use optic,[9–11] electro-optic,[13] and optoelectronic[14,15] devices. However, the use of all-electronic devices is desirable because electronic components are inexpensive and compact. Some recent efforts have started to address the issue of all-electronic generation of chaos in technologically relevant radio frequency bands.[16–20] For example, low dimensional chaos in the very-high-frequency range (30–300 MHz) has been demonstrated in a time-delay system with a diode-based nonlinearity.[18] It was also shown that Colpitts oscillators can generate chaos at GHz frequencies[19] and a high-speed chaotic delay-system with a transistor-based nonlinearity was reported.[20]

In this paper we describe an electronic time-delay feedback device that generates chaos in the very-high and ultra-high (0.3–3 GHz) frequency band. It is built using inexpensive commercially-available components such as ac coupled amplifiers and a transistor-based nonlinearity. Our device is similar to the one described by Mykolaitis *et al.*[20] However, in contradistinction to their work, we do not neglect, in modeling, the fact that rf components are ac coupled and we provide a detailed comparison of experimentally observed dynamics and the dynamics of the deterministic model of the device.

In our chaos generator, the complexity of the dynamics is controlled by feedback strength and time delay, allowing the device to be tuned from steady-state behavior, to periodic, quasiperiodic, and chaotic dynamics. The characteristic time scale of the dynamics can be tuned by adjusting the pass-band characteristics of the feedback loop. We chose to

[a]Electronic mail: illing@phy.duke.edu

work with feedback characteristics resulting in oscillations of several hundred MHz to a few GHz because this allows detailed measurements and characterization of the device dynamics. However, the device can, in principle, operate at higher frequencies, such as the 3–10 GHz frequency band, by using readily available higher-bandwidth components.

In modeling the device, we pay special attention to the fact that components are ac coupled, which means that low-frequency signals are suppressed. The time-delayed feedback is bandpass filtered because, in addition to the cutoff at low frequencies, high frequencies are suppressed due to the finite response time of device components.

The goal of this paper is to present details about the experimental implementation and to compare measurements and theory[21] to demonstrate that many aspects of the device dynamics can be explained if the band-limiting characteristic of the feedback is taken into account.

II. EXPERIMENTAL SETUP

It is well known that time-delayed feedback of the output signal of a nonlinearity to its input can give rise to chaotic dynamics.[13,15,16,20,22–24] Our rf-chaos generator is based on the same principle and we describe and characterize the device in this section. We discuss separately the passive nonlinearity, the setup of the rf-chaos generator, and the characteristics of the band-limited feedback with variable feedback gain.

A. Nonlinearity

The transistor-based nonlinearity consists of a bias-T and a modified Mini-Circuits ERA-SM test board (ERA-TB). The ERA-TB is a commercially available proto-board that is meant to test Mini-Circuits ERA amplifiers. A photograph of the modified ERA-TB is shown in Fig. 1(a) and the circuit diagram of the nonlinearity is shown in Fig. 1(b).

To create a nonlinear input-output relationship, the ERA-TB is modified by replacing the ERA-amplifier with a transistor (T1), capacitor (C1), and resistors (R_{NL} and R1) [Fig. 1(b)]. For this initial experiment, these components are placed using a "dead bug design," i.e., keeping them as close together as possible to avoid undesired feedback [white box in Fig. 1(a)].

The dc bias capabilities of the ERA-TB are used to set the power-supply voltage associated with the collector of transistor T1 [Fig. 1(b)] while ensuring, at the same time, good isolation of the rf-output signals and the dc-voltage part of the circuit. A variable bias voltage of the transistor base is achieved by further modifying the ERA-TB through removal of the ac-coupling capacitor at the input port and replacing it by an external bias-T, which combines the rf-input signal and the dc-bias voltage V_B. The bias voltage is $V_B=0.55$ V for all data shown in this paper, i.e. it is below the turn-on voltage V_T of the transistor (nominally $V_T\sim 0.7$ V).

To develop a simple model of the nonlinearity, consider the generated output as a function of input signals of sufficiently high frequency such that the effects of the coupling capacitors can be neglected. In this case, the output current is given by the voltage drop across the resistor R_{NL} for input voltages smaller than the difference of the turn-on voltage and the bias voltage (V_T-V_B) because the transistor draws essentially no collector current. In contrast, the output current is given by the difference of the current flowing through R_{NL} and the collector current of the transistor for input voltages larger than (V_T-V_B). This suggests a piecewise linear $I-V$ characteristic, which results in a corresponding piecewise linear input-voltage to output-voltage relationship assuming a standard 50 Ω load (the input impedance of the device coupled to the output port is assumed to be 50 Ω).

To determine the input-output characteristic of the nonlinearity experimentally, we inject a sinusoidal signal ($\nu=13$ MHz) into the input port of the nonlinearity and simultaneously recorded input and output using an oscilloscope (Agilent Infiniium, with 50 Ω input impedance, 2.25 GHz bandwidth, and 8 GSa/s). The measured tent-map-like input-output characteristic is shown as dots in Fig. 1(c). It is seen that the output depends linearly on the input for large input powers and that the nonlinearity has a smooth transition from positive to negative slopes. That is, a strictly piecewise-linear relation of input and output is a clear oversimplification of the actual nonlinearity. Furthermore, device models in which the nonlinearity is approximated as piecewise-linear do not reproduce several dynamic features of the experiment such as Hopf bifurcations, which are observed in the experiment but do not exist in a model with strictly linear segments. For this reason, we adopt the following phenomenological description of the nonlinearity:

$$F(v) = V_0 - \sqrt{F_1(v)^2 + a^2} \quad \text{with } F_1(v) = \begin{cases} A_l(v - v^*) & \text{if } v \leqslant v^*, \\ A_r(v - v^*) & \text{if } v > v^*. \end{cases} \tag{1}$$

Here, v denotes the input voltage, $v^*=V_T-V_B$ is the threshold voltage, and V_0 is an offset voltage. The slopes of F approach, respectively, A_l and A_r for large $|v|$ and the parameter a determines the sharpness of the peak of F.

In Fig. 1(c), a fit of Eq. (1) to the data is shown as a solid line, with fitted parameters $A_l=0.47$ (±0.04), $A_r=-0.62$ (±0.05), $a=0.05$ (±0.01) V, and $v^*=0.12$ ±0.04 V. Least-square minimization is used for fitting and a crude estimate of the sensitivity of the fit (values in brackets) is obtained by varying each parameter value individually and determining the size of parameter deviations above which the resulting input-output curve was clearly inconsistent with the data. The fit value of v^* suggests a transistor turn-on voltage of $V_T=0.67$ (±0.04 V), which is within the expected range. Also, the measured values of the slopes agree reasonably well with their expected values. As an example, one expects $A_l\sim R_L/(R_{NL}+R_L)=0.42$, where $R_L=50$ Ω is the load impedance and R_{NL} is nominally 68 Ω.

The correct value for the remaining parameter V_0 cannot be obtained from the data because the measured output signal is high-pass filtered by the coupling capacitor C2 [Fig. 1(b)]. As a result of the filtering, the measured output signal has a time average of zero, which, in terms of the filter-free input-output description of Eq. (1), implicitly determines the value of V_0 for a given input, thereby making the fit value of V_0 dependent on the properties of the input signal. For fur-

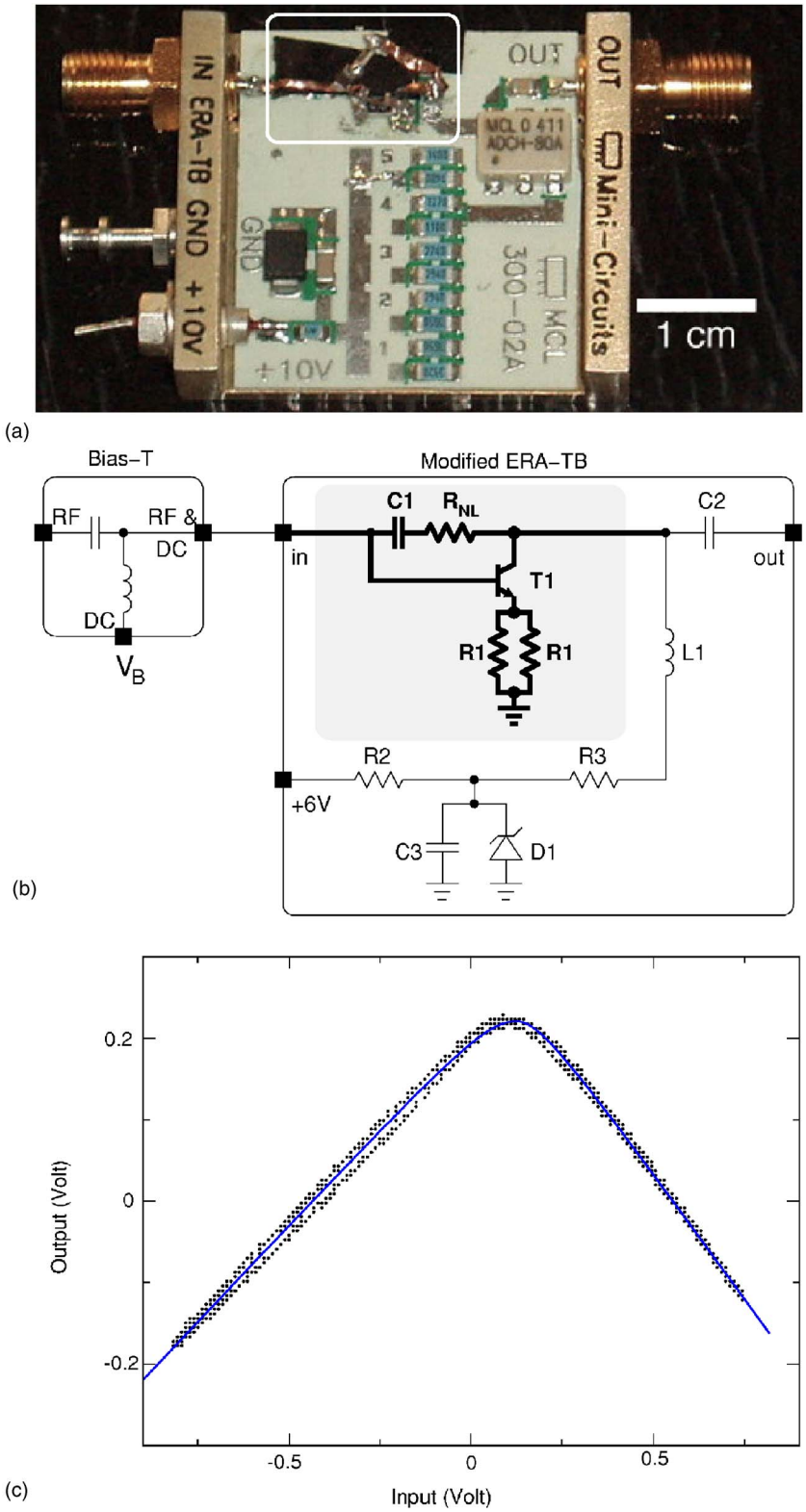

FIG. 1. Transistor-based nonlinearity. (a) Picture of the modified ERA-SM test board (modifications highlighted by the white box). (b) Details of the implementation of the nonlinearity, which consists of a bias-T (Mini-Circuits ZFBT 6GW, 0.1 MHz–6 GHz bandwidth) and a modified ERA-SM test board (Mini-Circuits ERA-TB). The component values on the ERA-TB are: C1=47 nF; C2 =0.39 μF; C3=0.1 μF; R_{NL}=68 Ω; R1=47 Ω; R2=4.75 Ω; R3=70 Ω; L1 is a rf choke (MCL Model AdcH-80A); D1 is a 10 V Zener diode; and T1 is an NPN 9 GHz wideband transistor BFG520. (c) Measured nonlinearity (dots) and fit of Eq. (1) (line).

ther modeling purposes, the knowledge of a precise value for V_0 is not necessary because the model also includes a high-pass filter [see Eq. (5)]. We set V_0=6 V in numerical simulations.

To test the frequency dependence of the nonlinearity, we vary the frequency of the sinusoidal injection signal. For frequencies up to 100 MHz, the input-output characteristics are essentially identical to that shown in Fig. 1(c). Beyond 100 MHz noticeable distortions arise mainly due to low-pass filtering in the nonlinearity and the measurement setup. Nevertheless, we believe that Eq. (1) is a valid description of the input-output characteristic for all experimentally relevant frequencies (3 MHz–1 GHz) in particular since the dynamic device model also includes a low-pass filter [see Eq. (5)].

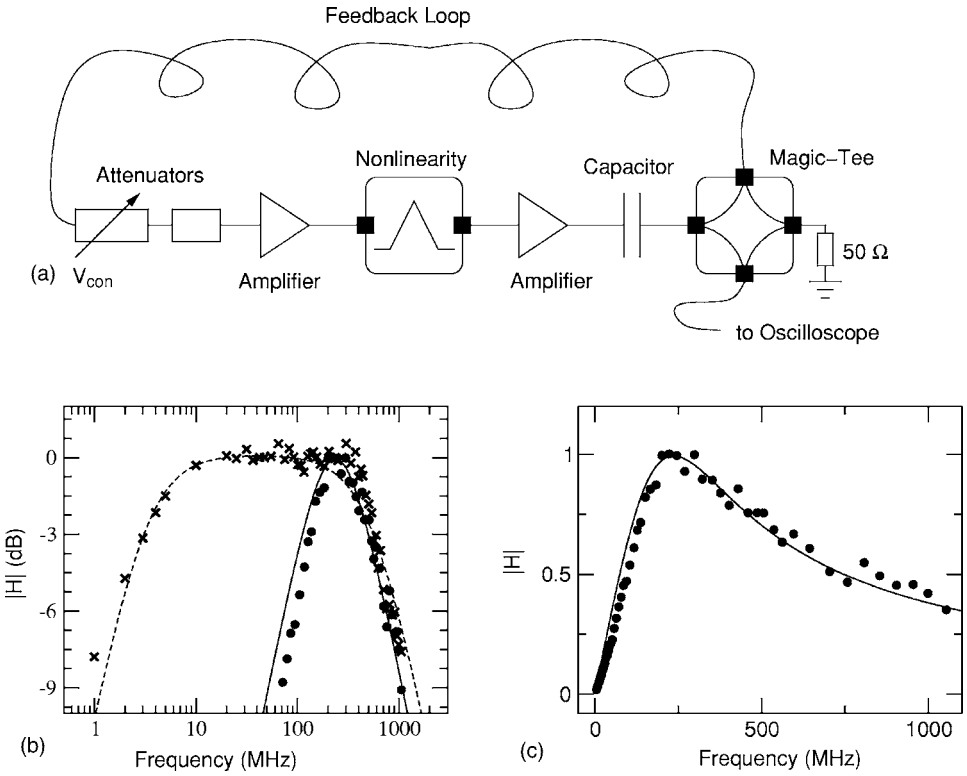

FIG. 2. An electronic generator of rf chaos. (a) Schematic of the device. (b) Transfer function $|H(\nu)|$ for the case of a 10 pF capacitor in the feedback loop (●: data; — fit) and without capacitor (×: data; - - -: fit). (c) Linear-scale plot of $|H|$ for the case of a 10 pF capacitor in the feedback loop (●: data; —: fit).

B. rf-chaos generator

To generate chaos, linear and amplified time-delayed feedback from the nonlinearity to itself is implemented as shown schematically in Fig. 2(a). In this device, the signal coming from the feedback loop passes through a voltage-tunable attenuator (Mini-Circuits ZX73-2500, bandwidth 10 MHz–2.5 GHz), a 12 dB fixed attenuator (JFW Industries Inc. 50HF-012, bandwidth dc-18 GHz), and a fixed-gain amplifier (Mini-Circuits ERA 5SM, bandwidth 60 kHz–4 GHz), which, in combination, results in a tunable amplification of the signal. The amplified signal passes through the nonlinearity, another fixed-gain amplifier (Mini-Circuits ERA 3SM, bandwidth 60 kHz–3 GHz) and is subsequently high-pass filtered by a capacitor (e.g., 10 pF). The filtered signal is then inverted and split by a hybrid magic-tee (M/A-COM H-9, bandwidth 2 MHz–2 GHz). Half the signal power is used for feedback and the other half is used as output. The output is recorded with an oscilloscope (Agilent Infiniium, with 50 Ω input impedance, 2.25 GHz bandwidth, and 8 GSa/s). All connections are made using SMA connectors and sufficient isolation of dc and ac signals is provided by the wideband rf-chokes (MCL Model ADCH-80A) contained in the biasing circuits for the amplifiers (Mini-Circuits ERA-TB). The total feedback-delay in our experiment is between 6 and 25 ns and can be varied on a coarse scale by changing the length of the coaxial-cable connecting the magic-tee and the attenuator [see Fig. 2(a)] or on a finer-scale by using a line stretcher (Microlab/FXR SR-05N 500 MHz−4 GHz) in the feedback (not shown).

C. Band-limited feedback with variable gain

To determine the transfer characteristics of the feedback, the coaxial cable that is attached to the output of the magic-tee [Fig. 2(a)] is disconnected and a small-amplitude sinusoidal signal is injected into the cable. Simultaneous measurement of input and output signals for different frequencies allows the determination of the transfer function $|H| = |V_{\text{out}}|/|V_{\text{in}}|$. The tent-map-like nonlinearity does not adversely affect this measurement because small-amplitude input signals ($V_{\text{in}}^{\text{rms}} < 100$ mV) only probe the "left" linear segment of the nonlinearity [see Fig. 1(c)].

The result of such a measurement of $|H|$ is shown in Fig. 2(b) on a log-log scale for a setup with a 10 pF capacitor in the feedback loop (●) and for a setup without a capacitor in the feedback loop (×). In the latter case, the high-pass filtering is entirely due to the fact that the rf components in the device are ac coupled. It is seen that the high-frequency cutoff is not affected by the inclusion of the 10 pF capacitor, whereas the high-pass filtering due to the capacitor shifts the low-frequency cutoff considerably.

To make contact with theory,[21] we fit the data shown in Fig. 2(b) to a model, where, for simplicity, the transfer characteristics of the feedback is approximated by a two-pole bandpass filter,

$$|H(\nu)| = \frac{\nu\delta}{\sqrt{(\nu_0^2 - \nu^2)^2 + \nu^2\delta^2}}. \tag{2}$$

Here, ν_0 denotes the frequency of maximal transmission and δ denotes the bandwidth. These parameters are given in terms of the 3 dB cutoff frequencies ν_+ and ν_- ($|H(\nu_\pm)|^2 = 1/2$) by $\nu_0^2 = \nu_+\nu_-$ and $\delta = \nu_+ - \nu_-$. For the case of a 10 pF capacitor in the feedback loop, the fit yields $\nu_0 \sim 236$ MHz and $\delta \sim 391$ MHz [$\nu_- = 110$ MHz, $\nu_+ = 502$ MHz, solid line in Figs. 2(b) and 2(c)]. For the case without an additional capacitor, $\nu_0 \sim 41$ MHz and $\delta \sim 547$ MHz is obtained [$\nu_- = 3$ MHz, $\nu_+ = 550$ MHz, dashed line in Fig. 2(b)]. In fitting,

we add more weight to data points with large values of $|H|$ because a good fit of the peak of $|H|$ is important for reproducing the observed dynamics.

Figures 2(b) and 2(c) show that a two-pole bandpass filter description of the transfer function is not a perfect approximation of the measured transfer characteristics. Clearly, allowing higher order filters would result in a better fit of the data. However, a description by higher-order filters would increase the model-complexity and we believe that the two-pole-filter approximation is a good compromise between model accuracy and model simplicity. Indeed, we will show below that quantitative agreement of theory and experiment is possible with this approximation.

The measured high-frequency 3 dB cutoff of 500–600 MHz is mainly due to the band-limitations of the nonlinearity (Fig. 1), for which a 3 dB cutoff frequency of ~1 GHz was measured. The bandwidth is further suppressed due to the combined effect of the nonideal behavior of the remaining device components [Fig. 2(a)], all of which exhibit a slow roll-off of the transfer function for frequencies below their 3 dB cutoff ($\geqslant$2 GHz). Higher bandwidths could be achieved in a future design by reducing the number of components and by implementing the nonlinearity as a microstrip circuit.

Another important parameter that characterizes the device is the feedback gain. It is varied, in the experiment, by changing V_{con}, the control voltage of the variable attenuator [Fig. 2(a)]. The dependence of the small-signal feedback gain on V_{con} was determined using the same setup that was used to measure $|H|$, only this time the frequency of the input signal is fixed at the frequency of maximal transmission ν_0 and V_{con} is varied. What is measured in this way is the small-signal effective gain at ν_0, denoted by b

$$b(V_{\mathrm{con}}) = -\gamma(V_{\mathrm{con}})F'(0). \tag{3}$$

Here, $\gamma(V_{\mathrm{con}})$ is the total feedback gain (non-negative), the minus sign accounts for the signal inversion at the magic-tee, and F' is the slope of the nonlinearity. The measured mapping of V_{con} to b is approximately linear for the control voltages used in the experiment (2–4 V) and is given by

$$b(V_{\mathrm{con}}) = -\beta(V_{\mathrm{con}} - V_0)e^{-\kappa\ell} \tag{4}$$

with $\beta = 1.195 \pm 0.002\ \mathrm{V}^{-1}$ and $V_0 = 1.15 \pm 0.02$ V. The exponential factor on the right-hand side of Eq. (4) takes into account signal attenuation in the coaxial cable, where ℓ is the length of the RG-174/U cable and $\kappa = 0.05\ \mathrm{m}^{-1}$.

III. MODEL AND THEORETICAL PREDICTIONS

In this section, we present a model and recall some theoretical results concerning steady-state bifurcations in delay-system with band-limited feedback.

Dynamics arises in the device due to the interaction of the nonlinearity and the linear time-delayed feedback. The complexity of models for such delay-feedback systems increases as more details about the feedback characteristics are included. For example, assuming a linear feedback of infinite bandwidth results in map-models, whereas taking into account the finite response time of device components through a single-pole low-pass filter results in scalar delay-differential equations.[22,23] It has been shown that for rf devices, such as the one discussed in this paper, it is essential to account for both the finite-bandwidth of the device-components (low pass filter) and the fact that rf components are ac coupled (high pass filter), in order to reproduce the observed dynamics at least qualitatively.[15,21,24] Thus, we adopt a model consisting of an integro-differential equation with time delay, where, for simplicity, it is assumed that the transfer characteristics of the feedback can be approximated by a two-pole bandpass filter:

$$v(t) + \frac{\dot{v}(t)}{\Delta} + \frac{\omega_0^2}{\Delta}\int_0^t dl v(l) = \alpha F\left[-\frac{\gamma}{\alpha}v(t-\tau)\right]. \tag{5}$$

In this equation, τ is the delay, ν is the bandpass filtered signal that is measured in the experiment, the parameter $\omega_0 = 2\pi\nu_0$ is the angular-frequency of maximal transmission, and $\Delta = 2\pi\delta$. For the case of a 10 pF capacitor in the feedback, $\omega_0 = 1.5\times10^9$ rad/s and $\Delta = 2.5\times10^9$ rad/s. The nonlinearity F is given by Eq. (1) and the minus sign in the argument of F in Eq. (5) accounts for the inversion of the feedback signal in the magic-tee. That is, the device has negative feedback. The parameter γ denotes the total feedback gain, whereas $\alpha \sim 9$ is the fixed gain a signal experiences between the output of the nonlinearity and the output of the magic-tee that is connected to the oscilloscope [see Fig. 2(a)].

Of the model parameters, ω_0 and Δ are known, the delay τ can be measured directly, and the total gain γ is determined in terms of the attenuator control voltage V_{con} by Eqs. (3) and (4) for the case of small amplitude dynamics. Thus, there are no free-parameters in the model and, consequently, quantitative predictions are possible.

In a previous publication, we analyzed the steady-state bifurcations for time-delay systems with band-limited feedback and arbitrary nonlinearity.[21] This analysis applies directly to the device model Eq. (5). The theory predicts that oscillations arise through Hopf bifurcations of the steady state and that the frequency of the oscillations at onset roughly scale as $\nu = n/(2\tau)$, where n is an odd integer for negative feedback. As a consequence of ac coupling, there exist jumps in the value of ν as a function of the delay, a feature that distinguishes bandpass feedback from low-pass feedback (Ikeda-type systems[22]). Furthermore, the theory predicts that the stability boundary of the steady state shows a lobe-like structure when plotted in the $b-\tau$ parameter plane.

The Hopf-bifurcation-type can also be determined. To that avail, note that the effective gain b is negative due to the negative feedback [Eq. (3)] and that the first and third derivative of the nonlinearity evaluated at the steady state satisfy $F'F''' < 0$ [Eq. (1)]. We show in the Appendix (Corollary 1) that, under these conditions, it follows from Illing and Gauthier[21] that the Hopf bifurcation is supercritical for delays satisfying

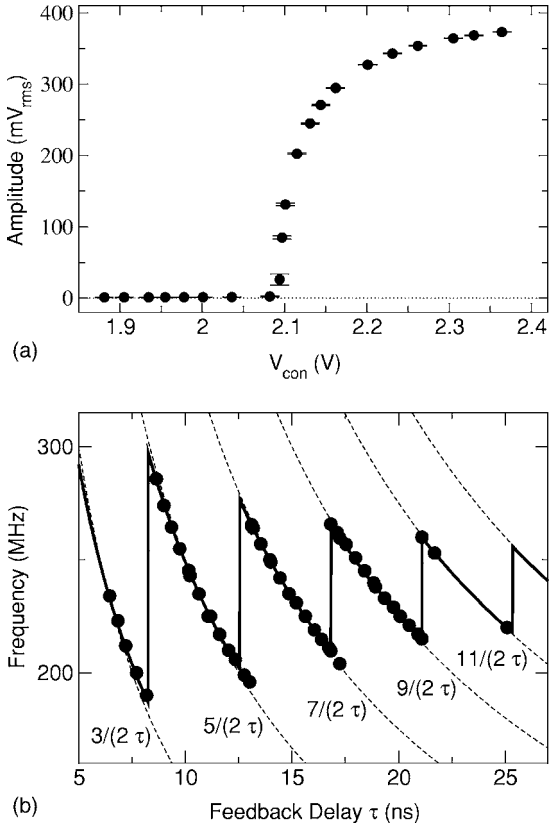

FIG. 3. Characterization of the Hopf bifurcations for a setup with a 10 pF capacitor. (a) Supercritical Hopf bifurcation: oscillation amplitude as a function of the attenuator control voltage V_{con} for $\tau=10.4$ ns. Increased V_{con} corresponds to increased (negative) feedback gain. (b) The measured dependence of the Hopf frequency on the time delay τ is shown (●). The dashed lines are the approximate $n/(2\tau)$ scaling. The solid line is from theory (see text).

$$\tau \geqslant \frac{\tau_C^1(2\pi/3)}{2\pi\delta} = \frac{1}{12}\frac{\delta}{\nu_0^2}(\sqrt{3+4\nu_0^2/\delta^2}-\sqrt{3}), \tag{6}$$

as long as $\nu_0^2/\delta^2 \leqslant 6$ holds. In particular, for the case of a 10 pF capacitor in the feedback loop, the model predicts the Hopf bifurcations to be supercritical for $\tau > 0.22$ ns, i.e., for all experimentally accessible delays.

IV. HOPF BIFURCATIONS

In this section, we compare experiment and theoretical predictions regarding the steady state bifurcation.

In experiment, we observe the dynamics of the device as we vary the feedback gain while the delay is held fixed. The feedback gain is increased by increasing the control voltage V_{con} of the tunable attenuator, i.e., by decreasing the attenuation. For small values of the feedback gain, the system resides in a steady state. As the gain crosses a critical value, a supercritical Hopf bifurcation occurs and gives rise to periodic oscillations.

An example of such a measurement is shown in Fig. 3(a), where it is seen that the oscillation amplitude grows smoothly as V_{con} is increased beyond a critical value of $\sim$2.1 V. In contrast, the measured oscillation frequency remains roughly constant ($\nu \sim 240$ MHz). In combination, these measurements indicate that the steady state loses stability through a supercritical Hopf bifurcation. We find that the steady state becomes unstable through supercritical Hopf bifurcations for all delays (6–25 ns), in agreement with the theoretical predictions.

An important advantage of chaos generators that use band-limited feedback is the ability to tune the main time scale of the device dynamics. In our device, the main time scale can be varied by more than a factor of 10 simply by changing the capacitor in the feedback loop (see Fig. 2). For example, at a fixed feedback delay of $\tau=10.5$ ns, the frequency is $\nu=48$ MHz for a setup without an additional capacitor in the feedback loop, $\nu=238$ MHz for $a\sim 10$ pF capacitor, and $\nu=913$ MHz for $a\sim 2$ pF capacitor. Here, we are using the frequency of the oscillations at the Hopf bifurcation (Hopf frequency) as a proxy for the main time scale.

Experimentally, the Hopf frequency is the quantity most readily measured and therefore ideally suited for comparison of experiment and theory. For all quantitative comparisons, we use an experimental setup with a 10 pF capacitor in the feedback. As a result, the main time scale of the dynamics is $\sim$4 ns ($=\nu_0^{-1}$), which allows high-resolution measurements in the time and frequency domain with the available equipment. Choosing ν_0 does not entirely fix the oscillation frequency at the Hopf bifurcation, which also depends on the time delay, as is shown in Fig. 3(b). It is seen that jumps occur between oscillation modes and that each mode scales as $\nu=n/(2\tau)$ with n odd (dashed lines), as predicted by the theory. The solid line in Fig. 3(b) is the result from a linear stability analysis of Eq. (5).[21] The agreement of theory and experimental data (●) in terms of the values of the Hopf frequency and the location of the mode jumps is excellent.

Another useful way to compare experiment and theory is to study the values of the feedback gain for which the steady state loses stability. Experimentally, an indirect measure of the critical feedback gain is obtained by measuring the attenuator control voltage V_{con} at the bifurcation for different delays τ. Figure 4(a) shows the result of such a measurement where the region of stability is shaded and an indication of the expected lobe-like structure of the stability boundary is discernible.

Theoretically, it is possible to predict the values of the feedback gain for which Hopf bifurcations occur by using the fitted values of ω_0 and Δ and linear-stability analysis of Eq. (5).[21] The result of such an analysis is shown in Fig. 4(b), where the solid line represents the critical values of the effective gain b plotted as a function of the delay τ. For comparison, we use Eq. (4) to map the measured values of V_{con} onto the corresponding b values and find very good quantitative agreement of theory and experiment.

However, we note that comparing the theory and experiment using frequency measurements is far more robust than the comparison based on the critical feedback gain because the frequency can be measured directly and with high precision whereas the effective gain b is determined indirectly through measuring V_{con} and using Eq. (4). Indeed, the error bars in Fig. 4(b) are mainly due to the $\sim$2% uncertainty of the fit parameter V_0 in Eq. (4). Another indication of the precision to which the mapping of V_{con} to b has to be known is the need to include the exponential factor in Eq. (4). This

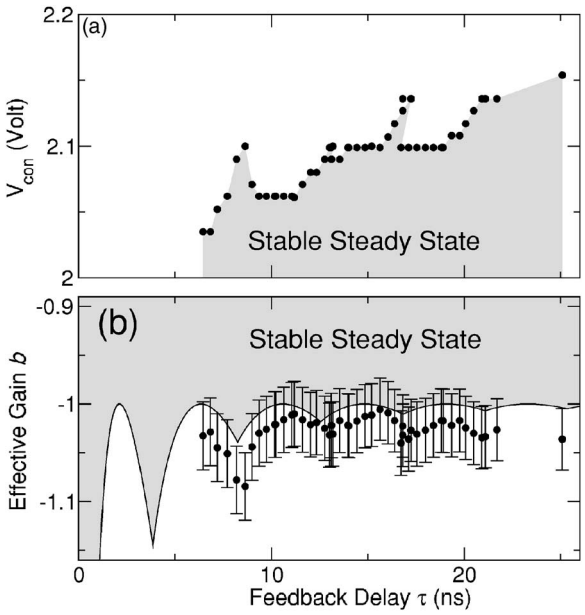

FIG. 4. Stability boundary of the steady state. (a) Experiment: measured attenuator control voltage V_{con} vs the feedback-delay τ. (b) Comparison of experiment and theory: values of V_{con} from panel (a) are mapped onto the effective slope b (●). The line indicates the theoretical prediction.

factor takes into account the small changes in signal attenuation that are the consequence of τ being varied by changing lengths of cable. Even these small changes in attenuation have noticeable effects, such as the increase, on average, of the critical value of V_{con} for increased delays [Fig. 4(a)].

In this section we have compared the experimentally measured device dynamics to analytic predictions based on a parameter-free model consisting of a simple integro-differential equation with time delay. On the level of bifurcations from the steady state, such a simple model turns out to be sufficient to reproduce the observed dynamics quantitatively.

V. HIGH-DIMENSIONAL CHAOS

Beyond the Hopf bifurcation, successively more complex dynamics develop as the gain is increased. Experimental results are presented in Fig. 5, where time traces are displayed in the first column and the corresponding spectra in the second column. In the third column, we show the location where the measured trajectory crosses unidirectionally a Poincaré plane in a three-dimensional delay-embedding space with embedding-delay $\Delta_\tau = 1$ ns. At feedback gains slightly above the critical value, the oscillations are sinusoidal [Fig. 5(a)], resulting in a spectrum that is dominated by the main frequency [Fig. 5(b)] and a single point in the Poincaré plane [Fig. 5(c)]. At higher feedback gains, the oscillations begin to square off and prominent odd harmonics appear in the spectrum (not shown). As the gain is increased further, frequency components that are noncommensurate with the fundamental frequency appear and grow in power, resulting in a dense comb of frequencies in the spectrum. This signature of quasiperiodic dynamics is clearly seen in Fig. 5(e). The existence of a torus attractor is confirmed by the appearance of a closed curve in the Poincaré section [Fig. 5(f)]. For even larger gains, the broad background in the spectrum rises and the power in the fundamental frequency peak shrinks, as can be seen in Fig. 5(h). Furthermore, no structure can be discerned in the Poincaré section. This is indicative of high-dimensional chaos.

We use numeric simulations to show that model (5) reproduces the observed dynamics of the device qualitatively and we substantiate the claim of high-dimensional chaos by demonstrating that the deterministic model is chaotic.

Figure 6 shows time series, power spectra, and Poincaré sections obtained by numerical simulation[25] of Eq. (5) (compare with Fig. 5). We find sinusoidal oscillations [Figs. 6(a)–6(c)] for $\gamma = 2.8$ ($b = -1.01$). This value of γ corresponds to $V_{con} = 2.07$ V and is obtained by using Eqs. (3) and (4). For the large amplitude oscillations that arise in the experiment for $V_{con} = 2.6$ V ($V_{con} = 3.6$ V) saturation effects start to

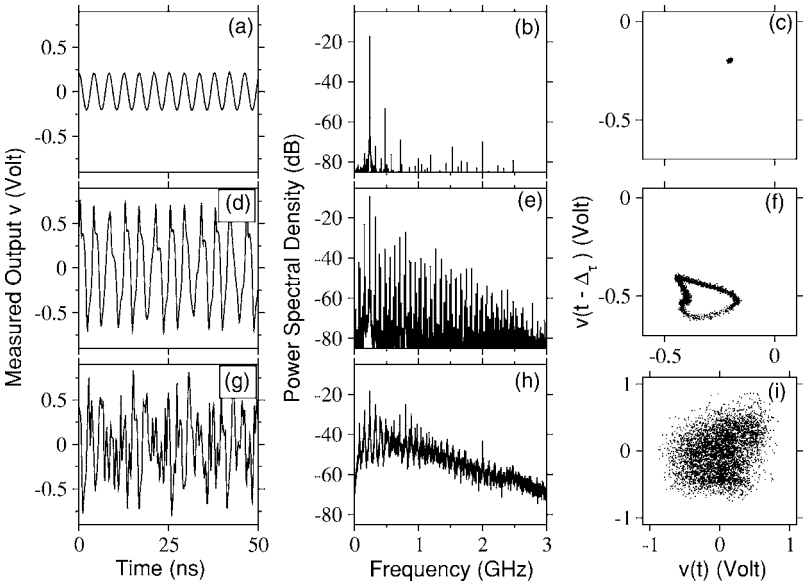

FIG. 5. Experimentally measured time series as well as the corresponding power spectra and Poincaré sections are shown for (a)–(c) $V_{con} = 2.07$ V, (d)–(f) $V_{con} = 2.6$ V, and (g)–(i) $V_{con} = 3.6$ V. The feedback loop contained a ~10 pF capacitor, $\tau = 10.5$ ns, and $\Delta_\tau = 1$ ns.

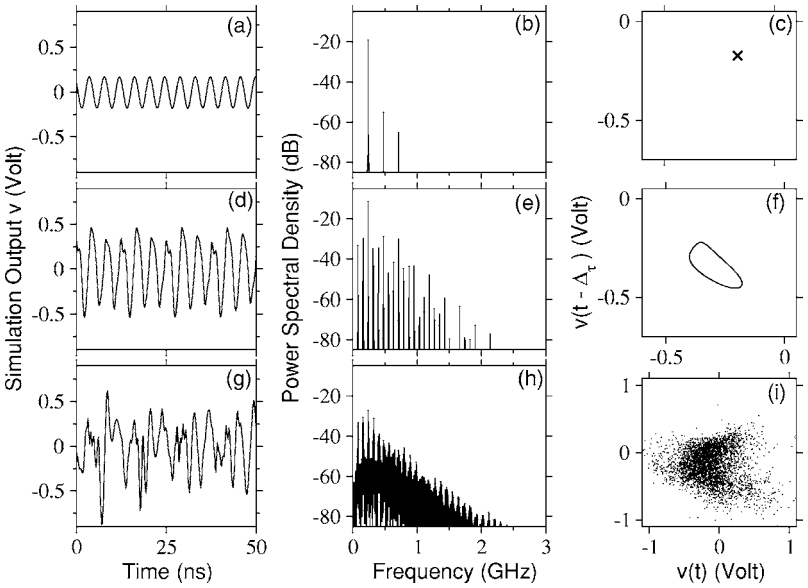

FIG. 6. Numerical time series, power spectra, and Poincaré sections (Δ_τ=1 ns) are shown for (a)–(c) γ =2.8, (d)–(f) γ=3.7, (g)–(i) γ=4.5 ($D_L \sim 13$).

play a role and based on measurements we estimate the corresponding gain to be $\gamma \sim 3.7$ ($\gamma \gtrsim 6$). Increasing the feedback gain in the simulations to γ=3.7 confirms that the limit cycle bifurcates to a torus-attractor as shown in Fig. 6(f) by the closed curve in the Poincaré section. The power spectrum [Fig. 6(e)] exhibits a comb-like structure due to the two incommensurate frequencies of the quasiperiodic oscillation. For even larger gains the system is chaotic, with a very broadband spectrum [Fig. 6(h)] and no discernible structure in the Poincaré section [Fig. 6(i)]. We computed Lyapunov exponents for the model with γ=4.5 and find that the largest few exponents are positive.[26] This proves that the model dynamics shown in Fig. 6(g) are on a chaotic attractor. We estimate the attractor's Lyapunov dimension to be $D_L \sim 13$.

In this section, we have presented evidence that our device exhibits high-dimensional chaos. We have shown that the device can be tuned from steady state behavior to quasiperiodic dynamics, and aperiodic oscillations with a broad power spectrum. This behavior is reproduced by the deterministic model and we have quantified the dimensionality of the chaotic attractor.

VI. SUMMARY AND DISCUSSION

Time delays are present and signals are bandpass filtered in circuits that operate in the ultra-high frequency band and consist of commercially available prepackaged rf components. Our approach is to exploit inherent time delays and band-limiting component characteristics for the generation of complex dynamics. We discuss in this paper a device resulting from this approach, an easy to implement all-electronic generator of chaotic oscillations at GHz frequencies. The device has the advantage that the characteristic time scale and the bandwidth of the chaotic output can be tuned by changing the properties of the feedback loop. Further positive aspects of the device are that it is built using commercially-available components and that it can, in principle, be operated at higher frequencies such as the 3–10 GHz band in which the operation of ultra-wideband transmission systems is allowed.[27]

Comparison of the measured device dynamics to theory shows that a simple integro-differential equation with delayed feedback (equivalent to a second-order delay-differential equation) captures many of the observed dynamic features. Indeed, good quantitative agreement is found on the level of bifurcations from the steady state and the observed quasiperiodic and chaotic behavior is qualitatively reproduced by the model.

In this context, it is important to note that the device was operated in a "weak" feedback regime for all data shown in this paper. In the experimental device, the amplifiers will exhibit saturation effects for strong feedback, which introduces additional feedback nonlinearities. In the strong-feedback regime, we observe chaotic oscillations with a nearly featureless power spectrum (not shown). In contrast, the saturation-free model [Eqs. (1) and (5)] becomes unstable for large values of the feedback parameter γ ($\gamma \gtrsim 5$). However, omitting saturation effects in the model allows us to show conclusively that high-dimensional chaos arises in the weak-feedback regime due to the interaction of the linear band-limited time-delayed feedback with the transistor-based nonlinearity.

It is well known that dynamical systems with delayed feedback often have very rich dynamics and bifurcation diagrams. This is also true for delay systems with band-limited feedback. For example, we observe coexisting stable limit cycles over wide parameter ranges, demonstrating the system's multistability. Furthermore, periodic windows are found within the quasiperiodic and chaotic regimes, which is indicative of the complex bifurcation scenario in this system. It would be interesting to investigate in more detail the bifurcations leading to quasiperiodicity and to the appearance of periodic windows.

Numerical studies of time-delay systems suggest[28] that the Lyapunov dimension of the chaotic attractor grows with increased delay while the metric entropy stays roughly con-

stant. In our device, one would therefore expect to find low-dimensional chaotic behavior for small delays with a Lyapunov spectrum that has few but large positive Lyapunov exponents. This is confirmed in numerical simulations where we find that, for a short delay of $\tau=0.5$ ns, the Lyapunov dimension never rises above $D_L=3.5$ for all feedback strengths where model (5) is stable ($\gamma<7.8$). Furthermore, the Lyapunov spectrum has at most a single positive exponent with typical values of $\sim 1\ \mathrm{ns}^{-1}$. As a comparison, six positive exponents of size $\lesssim 10^{-2}\ \mathrm{ns}^{-1}$ are found for the large-delay case ($\tau=10.5$ ns, $D_L\sim 13$) shown in Fig. 6(g). Experimentally, we cannot access the short-delay regime with our current setup, which was designed to provide independent control over system parameters such as feedback-gain, time-delay, and transistor bias-voltage. As a result, our device consists of many components with the consequence that $\tau\gtrsim 6$ ns. In a future setup, it should be possible to operate the circuit in the short-delay regime by reducing the number of components and by combining them onto a single microstrip circuit.

We believe that this chaotic electronic device is ideally suited for both experimental investigation of the nonlinear dynamics of time-delay systems and technological application of high-speed chaos such as ranging, intrusion detection, tracking, and random number generation.

ACKNOWLEDGMENTS

We thank W. L. Ebenstein for helping us with the measurements. This work was supported by the U.S. Army Research Office Grant No. W911NF-05-1-0228.

APPENDIX: HOPF BIFURCATION TYPE

In a previous publication,[21] we have derived simple criteria that determine whether the Hopf bifurcation of the steady state is supercritical or subcritical. In our analysis we focus on large-bandwidth systems, i.e., systems where the quality factor $Q\leqslant 1/2$ ($Q=\omega_0/\Delta$). However, the rf device that is discussed in the current paper produces Hopf bifurcations and chaos for both large and small bandwidths. As an example, when there is no capacitor in the feedback loop the quality factor is $Q\sim 0.07$, whereas $Q\sim 0.6$ with a 10 pF capacitor in the feedback loop. The purpose of this section is to derive a simple condition for the Hopf bifurcation type that is valid for $Q>1/2$.

To that avail, we first show that Eq. (5) is equivalent to the second order delay-differential equation studied in Ref. 21. To do so, we introduce new variables $x=-(\gamma/\alpha)v$ and $y=-\gamma F[0]+(\omega_0^2\gamma)/(\Delta\alpha)\int_0^t v(l)dl$, rescale time through $s=t\Delta$ ($\hat{\tau}=\tau\Delta$), and define $r=\omega_0^2/\Delta^2$ as well as $f(x)=F(x)-F(0)$. As a result, we obtain

$$\dot{x}(s)=-x(s)+y(s)-\gamma f[x(s-\hat{\tau})],$$

$$\dot{y}(s)=-rx(s), \tag{A1}$$

which is precisely the model discussed in Ref. 21.

The main result concerning the Hopf-bifurcation-type, i.e. Proposition 2 in Ref. 21, is derived without using the assumption $r=Q^2\leqslant 1/4$. Therefore, the following holds:

Proposition 1: For $r,\hat{\tau}\in\mathbb{R}^+$ *and* $n=0,1,2,\ldots$:

If $f'(0)f'''(0)+f''(0)^2C^n(\hat{\tau},r)<0(>0)$, *the Hopf bifurcation is supercritical (subcritical).*

Here, $C^n(\hat{\tau},r)$ is a function that is given by Eq. (40) in Ref. 21 (the label n denotes the mode). Proposition 1 shifts the difficulty of determining the Hopf-bifurcation-type to knowing the value of $C^n(\hat{\tau},r)$ and it is clearly useful to derive conditions that determine the sign of $C^n(\hat{\tau},r)$. Inspection of the proof of Proposition 4 in Ref. 21 reveals that the following is true:

Proposition 2: For $r,\hat{\tau}\in\mathbb{R}^+$ *and* $n=0,1,2,\ldots$:

If $b\in[-2,-1]$, $C^n(\hat{\tau},r)<0$; *if* $b\in(1,2]$ *and* $\hat{\tau}>(n\pi)/\sqrt{r}$, $C^n(\hat{\tau},r)<0$; *and if* $b=1$, $C^n(\hat{\tau},r)=0$.

In terms of the experiment, we are mainly interested in the Hopf bifurcations of the *stable* steady state, i.e., in the bifurcation type at the stability boundary. A simple criterion that guarantees supercritical bifurcations at the stability boundary is obtained by determining the values of r for which the stability boundary is contained in the interval $|b|\in[1,2]$ for all $\hat{\tau}$.

The stability boundary in the $b-\hat{\tau}$ parameter plane is composed of pieces of Hopf curves [the parameterized curves $\{b_C^n(\cdot),\tau_C^n(\cdot)\}$ are given by Eqs. (14) and (15) in Ref. 21]. The steady state is stable for all delays, if $|b|<1$. For positive feedback ($b>0$), the maximum value of b for which the steady state is stable is given by the point in the $b-\hat{\tau}$ parameter plane where the Hopf curves of mode $n=0$ and $n=2$ intersect (double Hopf point). As r increases, this point moves to larger values of b and crosses $b=2$ for $r=15/16$. Similarly, for negative feedback and $\hat{\tau}\geqslant\tau_C^1(2\pi/3)$, the minimum b for which the steady state is stable is given by either $b_C^1(2\pi/3)=-2$ or the point where the Hopf curves of modes $n=1$ and $n=3$ intersect. As r increases, the double Hopf point moves to smaller values of b and crosses $b=-2$ for $r=6$. Thus, we obtain the following simple criteria for the Hopf-bifurcation-type (extending Corollary 5 in Ref. 21):

Corollary 1: At the stability boundary of the steady state, the following holds for the Hopf bifurcation: If $b<0$, $\hat{\tau}\geqslant\tau_C^1(2\pi/3)$, $r\leqslant 6$, *and* $f'(0)f'''(0)<0$, *the bifurcation is supercritical. If* $b>0$, $\hat{\tau}\geqslant n\pi/\sqrt{r}$, $r\leqslant 15/16$, *and* $f'(0)f'''(0)<0$, *the bifurcation of the nth mode from the steady state is supercritical.*

[Note the typographical error in Ref. 21, Corollary 5, point (3), the condition should read $\tau\geqslant\tau_C^1(2\pi/3)$.]

[1] T. Carroll and L. Pecora, *Nonlinear Dynamics in Circuits* (World Scientific, Singapore, 1995).
[2] K. Myneni, T. A. Barr, B. R. Reed, S. D. Pethel, and N. J. Corron, Appl. Phys. Lett. **78**, 1496 (2001).
[3] K. A. Lukin, *The Fourth International Kharkov Symposium on Physics and Engineering of Millimeter and Submillimeter Waves, Kharkov* (IEEE, Piscataway, 2001), p. 68.
[4] F. Y. Lin and J. M. Liu, IEEE J. Sel. Top. Quantum Electron. **10**, 815 (2004).
[5] F. Y. Lin and J. M. Liu, IEEE J. Sel. Top. Quantum Electron. **10**, 991 (2004).
[6] T. Stojanovski, J. Pihl, and L. Kocarev, IEEE Trans. Circuits Syst., I: Fundam. Theory Appl. **48**, 382 (2001).
[7] A. Gerosa, R. Bernardini, and S. Pietri, IEEE Trans. Circuits Syst., I: Fundam. Theory Appl. **49**, 993 (2002).
[8] J. T. Gleeson, Appl. Phys. Lett. **81**, 1949 (2002).
[9] G. D. VanWiggeren and R. Roy, Science **279**, 1198 (1998).

[10]I. Fischer, Y. Liu, and P. Davis, Phys. Rev. A **62**, 011801 (2002).
[11]K. Kusumoto and J. Ohtsubo, Opt. Lett. **27**, 989 (2002).
[12]V. Dronov, M. R. Hendrey, T. M. Antonsen, and E. Ott, Chaos **14**, 30 (2004).
[13]N. Gastaud, S. Poinsot, L. Larger, J. M. Merolla, M. Hanna, and J. P. Goedgebuer, F. Malassenet, Electron. Lett. **40**, 898 (2004).
[14]H. D. I. Abarbanel, M. Kennel, L. Illing, S. Tang, H. F. Chen, and J. M. Liu, IEEE J. Quantum Electron. **37**, 1301 (2001).
[15]J. N. Blakely, L. Illing, and D. J. Gauthier, IEEE J. Quantum Electron. **40**, 299 (2004).
[16]J. N. Blakely and N. J. Corron, Chaos **14**, 1035 (2004).
[17]V. Demergis, A. Glasser, M. Miller, T. M. Antonsen, Jr., E. Ott, and S. M. Anlage, http://arxiv.org/abs/nlin.CD/0605037
[18]J. N. Blakely, J. D. Holder, N. J. Corron, and S. D. Pethel, Phys. Lett. A **346**, 111 (2005).
[19]G. Mykolaitis, A. Tamaševičius, and S. Bumelienė, Electron. Lett. **40**, 91 (2004).
[20]G. Mykolaitis, A. Tamaševičius, A. Čenys, S. Bumelienė, A. N. Anagnostopoulos, and N. Kalkan, Chaos, Solitons Fractals **17**, 343 (2003).
[21]L. Illing and D. J. Gauthier, Physica D **210**, 180 (2005).
[22]K. Ikeda and K. Kondo, Phys. Rev. Lett. **49**, 1467 (1982).
[23]P. Celka, Physica D **104**, 127 (1997).
[24]V. S. Udaltsov, L. Larger, J. P. Goedgebuer, M. W. Lee, E. Genin, W. T. Rhodes, IEEE Trans. Circuits Syst., I: Fundam. Theory Appl. **49**, 1006 (2002).
[25]We numerically integrate Eq. (A1) using an Adams-Bashforth-Moulton predictor-corrector algorithm. The mapping of model (5) onto Eq. (A1) is given in the Appendix.
[26]Details on the computation of the Lyapunov spectrum can be found in Ref. 14.
[27]The Federal Communications Commission (FCC) revised the rules regarding ultra-wideband transmission systems in 2002 in order to permit the marketing and operation of ultra-wideband technology.
[28]J. D. Farmer, Physica D **4D**, 366 (1982).